metals

MDPI

Article

Influence of Sintering Temperature on the Structural, Morphological, and Electrochemical Properties of NiO-YSZ Anode Synthesized by the Autocombustion Route

Muneeb Irshad [1], Muhammad Rafique [2], Asif Nadeem Tabish [3], Abdul Ghaffar [4], Ahmad Shakeel [3,5,*], Khurram Siraj [1], Qurat ul Ain [1], Rizwan Raza [6], Mohammed Ali Assiri [7] and Muhammad Imran [7]

1 Department of Physics, University of Engineering and Technology, Lahore 54890, Pakistan; muneeb_irshad@uet.edu.pk (M.I.); ksiraj@uet.edu.pk (K.S.); quratulainquratulain786@gmail.com (Q.u.A.)
2 Department of Physics, University of Sahiwal, Sahiwal 57000, Pakistan; mrafique@uosahiwal.edu.pk
3 Department of Chemical Engineering, University of Engineering and Technology, Lahore 39021, Pakistan; antabish@uet.edu.pk
4 Department of Physics, Government College University (GCU), Lahore 54000, Pakistan; abdulghaffar@gcu.edu.pk
5 Department of Hydraulic Engineering, Faculty of Civil Engineering and Geosciences, Delft University of Technology, 2628 CN Delft, The Netherlands
6 Clean Energy Research Lab (CERL), Department of Physics, COMSATS University Islamabad, Lahore 54000, Pakistan; rizwanraza@cuilahore.edu.pk
7 Research Center for Advanced Materials Science (RCAMS), Department of Chemistry, Faculty of Science, King Khalid University, Abha 61413, Saudi Arabia; maassiri@kku.edu.sa (M.A.A.); miahmad@kku.edu.sa (M.I.)
* Correspondence: a.shakeel@tudelft.nl

Citation: Irshad, M.; Rafique, M.; Tabish, A.N.; Ghaffar, A.; Shakeel, A.; Siraj, K.; Ain, Q.u.; Raza, R.; Assiri, M.A.; Imran, M. Influence of Sintering Temperature on the Structural, Morphological, and Electrochemical Properties of NiO-YSZ Anode Synthesized by the Autocombustion Route. *Metals* **2022**, *12*, 219. https://doi.org/10.3390/met12020219

Academic Editor: Joan-Josep Suñol

Received: 27 November 2021
Accepted: 18 January 2022
Published: 24 January 2022

Abstract: In this study, nickel oxide–Y_2O_3-doped ZrO_2 (NiO-YSZ) composite powder as an anode material was synthesized using a cost-effective combustion method for high-temperature solid oxide fuel cell (SOFC). Further, the effects of sintering temperatures (1200, 1300, and 1400 °C) were studied for its properties in relation to the SOFC performance. The prepared and sintered NiO-YSZ materials were characterized for their surface morphology, composition, structure, and conductivity. The cubic crystalline nature of NiO and YSZ was sufficed by X-ray diffraction, and SEM images revealed an increase in the densification of microstructure by an increase in the sintering temperature. EDX spectrum confirmed the presence of nickel, yttrium, and zirconia without any impurity. Conductivity measurements, under a hydrogen environment, revealed that NiO-YSZ, sintered at 1400 °C, exhibits better conductivity compared to the samples sintered at lower temperatures. Electrochemical performance of button-cells was also evaluated and peak power density of 0.62 Wcm^{-2} is observed at 800 °C. The citrate combustion method provided peak performance for cells containing anode sintered at 1200 °C, which was previously reported at higher sintering temperatures. Therefore, the citrate combustion method is found to be a suitable route to synthesize NiO-YSZ at low sintering temperature.

Keywords: composite; autocombustion synthesis; sintering; microstructure; electrochemical performance

1. Introduction

Natural resources include oil, coal, natural gas, fossil fuel, etc., are being consumed to fulfill the world's increasing energy requirements. Customary fossil fuels are also counted as the main energy sources. However, there are critical environmental problems like water, air, and land pollution because of the non-renewable nature associated with fossil fuels. To fulfill the energy needs and tackle environmental issues, fuel cells can serve the purpose of being a clean, efficient, and sustainable energy source [1–3].

A fuel cell produces electrical energy from the chemical energy with higher efficiency and zero-emission. Solid oxide fuel cells (SOFCs) are preferred because of their higher efficiency, environment-friendly nature, internal reforming process, easy maintainability, excellent reliability, size and fuel flexibility, production of heat and power, etc. [4,5]. In most SOFCs, high temperatures (800–1000 °C) are a requisite for complete oxidation along with the chemical degradation and limitation of material selection, etc., as drawbacks. Reducing its operating temperature (600–800 °C) can affect the cost, stability, and choice of materials. Anode, cathode, and a dense electrolyte sandwich between electrodes are main constituents of SOFC [6,7]. An anode should exhibit high ionic and electronic conductivity, sufficient porosity, chemical stability, and suitable triple phase boundary (TPB), etc. The electrolyte is not susceptible to corrosion, because all the components of a SOFC are in the solid phase. Due to this advantage, it can be used as a portable electric generator in many disciplines such as cogeneration power plants, auxiliary power supplies, train and ship engines, distributed power supplies, etc. [6,8,9].

Nickel based anode materials are frequently used because of their better electronic and ionic conductivity, good catalytic activity, and cost-effectiveness. In the case of NiO (nickel oxide)–YSZ (Y_2O_3-doped ZrO_2, yttria-stabilized zirconia) based anode, nickel (after reduction) can easily oxidize different chemicals used as fuel, such as hydrocarbons, hydrogen, etc., and is responsible for the electronic transport to the external circuit [10,11]. The YSZ material not only supports the nickel particles but also takes part in ionic conduction and thermal expansion and is used to produce a proper networked structure necessary for the catalytic activity [12]. NiO, after reduction into Ni metal, plays a vital role to determine the structure and electronic conductivity of the anode. Sometimes periodic nucleation of metallic clusters takes place during the reduction of NiO in the hydrogen atmosphere. These clusters further develop into crystallites at an approximately linear rate. NiO reduction to Ni increases the porosity of the material, and as a result the solid volume reduces. After reduction, the cermet anode material consists of three interconnected phases: YSZ, nickel, and porosity. Here, porosity is an important factor for the diffusion of gas towards the triple-phase boundary and is significant for the SOFC overall performance [13]. At triple-phase boundary Ni, YSZ and gas interact with each other. For low nickel contents, the electronic conductivity will be very low and if its concentration is high then nickel aggregation occurs, causing a decrease in porosity, affecting the performance at the TPB. Therefore, the concentration of nickel must be in an appropriate range to avoid a mismatch of electrolyte and anode [14]. The total conductivity of NiO-YSZ anode is electronic owing to the proper arrangement of both NiO and YSZ phases. The electrical conductivity Ni(after reduction) is five times greater compared to ionic conductivity of the YSZ [15].

NiO-YSZ based anode materials are well known because of high porosity, high ionic and electronic conductivity, thermal expansion compatibility with other SOFC materials, and structural stability. The thermal expansion coefficient lies near the YSZ electrolyte, which improves performance by increasing the TPB [6,16]. When the Ni-YSZ based cermet anode (after reduction) comes in contact with the hydrocarbon fuel, then issues like carbon deposition, contamination, etc. also arise. The effect of aging on 40, 50, and 60 wt.% of Ni in 8 mol% YSZ after 500 h of heating has been studied, and it was found that only 40 wt.% Ni-YSZ exhibited a loss of metallic conductivity. In addition, through the sintering process, it has been noticed that electrical conductivity was not affected by the aging process [17].

Different synthesis routes have been employed to synthesize the NiO-YSZ anode, such as the modified glycine-nitrate, ball milling, hydrothermal, sol-gel technique, and mechanochemical route, etc. [16,18,19]. The main advantage of these synthesis approaches is that they produce a uniform nanostructure with high porosity without the need for a reformer. Hence, the choice of synthesis technique can shape the microstructure, mechanical, and electrical properties of the desired anode material. NiO-YSZ, when prepared by both mechanochemical and sol-gel methods, shows that the sol-gel route is superior for achieving a better crystalline structure, small size crystallite, high specific surface area, and uniform distribution of particles [18].

To date, a variety of methods are being used to produce NiO-YSZ material for SOFC applications. The purpose of this work is to highlight the combustion method as an easy, fast, and cost-effective method to synthesize NiO-YSZ material as a SOFC anode. Sintering is also performed at 1200, 1300, and 1400 °C to generate the desired structure-based effects necessary to improve the performance of SOFCs. Investigations over the crystal structure, surface morphology, thermal behavior, conductivity, and electrochemical performance of the prepared material are presented in this report. The electrochemical performance of NiO-YSZ synthesized by auto-combustion was studied.

2. Experimentation

The auto-combustion route was employed to synthesize the NiO-YSZ as anode material. Precursors, zirconium oxynitrate hydrate (99%, Sigma), nickel nitrate hexahydrate (99.99%, Sigma), yttrium nitrate hexahydrate (99.8%, Alfa Aesar), and citric acid (>99%, Sigma) were procured from Sigma-Aldrich and used without further treatment. The yttrium nitrate hexahydrate and zirconium oxynitrate hydrate were dissolved in distilled water and stirred for 30 min at 80 °C to form a homogenous mixture. An aqueous solution of nickel nitrate hexahydrate was added in this solution and stirred for 30 min for homogenization. Citric acid was added as a chelating agent into the prepared homogenized solution. The gel was formed under continuous heating and stirring. On further heating, this gel was burnt due to auto-ignition and combusted powder was obtained. The hypothesized chemical reaction between these materials is described as:

$$x[2\{Y(NO_3)_3{\cdot}6H_2O\}] + y[ZrO\ (NO_3)_2{\cdot}xH_2O] + 3[Ni(NO_3)_2{\cdot}6H_2O] + \ C_6H_8O_7 \rightarrow \ Y_2ZrO_5 + 3NiO + 9N_2 + 15O_2 + 6CO_2 + 30xH_2O. \quad (1)$$

The combusted powder was dried at 150 °C. The dried powder was grinded and sintered at 1200, 1300, and 1400 °C for 4 h. The obtained powder was then compacted into the pellet form using a hydraulic press at 200 MPa. The flow chart of the synthesis of NiO-YSZ is given in Figure 1.

Structural investigations of synthesized NiO-YSZ powder were done by X'pert pro super Diffractometer (Philips, Amsterdam, Netherland). The calculation of crystallite size was done through Bragg's peak analysis using the Debye-Scherer formula [20],

$$D = \frac{K\,\lambda}{\beta \cos\theta}, \quad (2)$$

Energy dispersive analysis was used to find elemental composition. Scanning electron microscopy, S-3000H (HITACHI, Tokyo, Japan) was used to examine the surface morphology.

Thermal analysis was performed by TA TGA Q500 (TA Instruments, New Castle, DE, USA). The electrical conductivity was observed through the four-probe method. The electrical conductivity was calculated by

$$\sigma = \frac{L}{R \times A}, \quad (3)$$

The Arhenius equation was employed to determine the temperature dependent conductivity and is given as [21]

$$\sigma = \frac{A}{T} \exp\left(-\frac{E_a}{K \times T}\right). \quad (4)$$

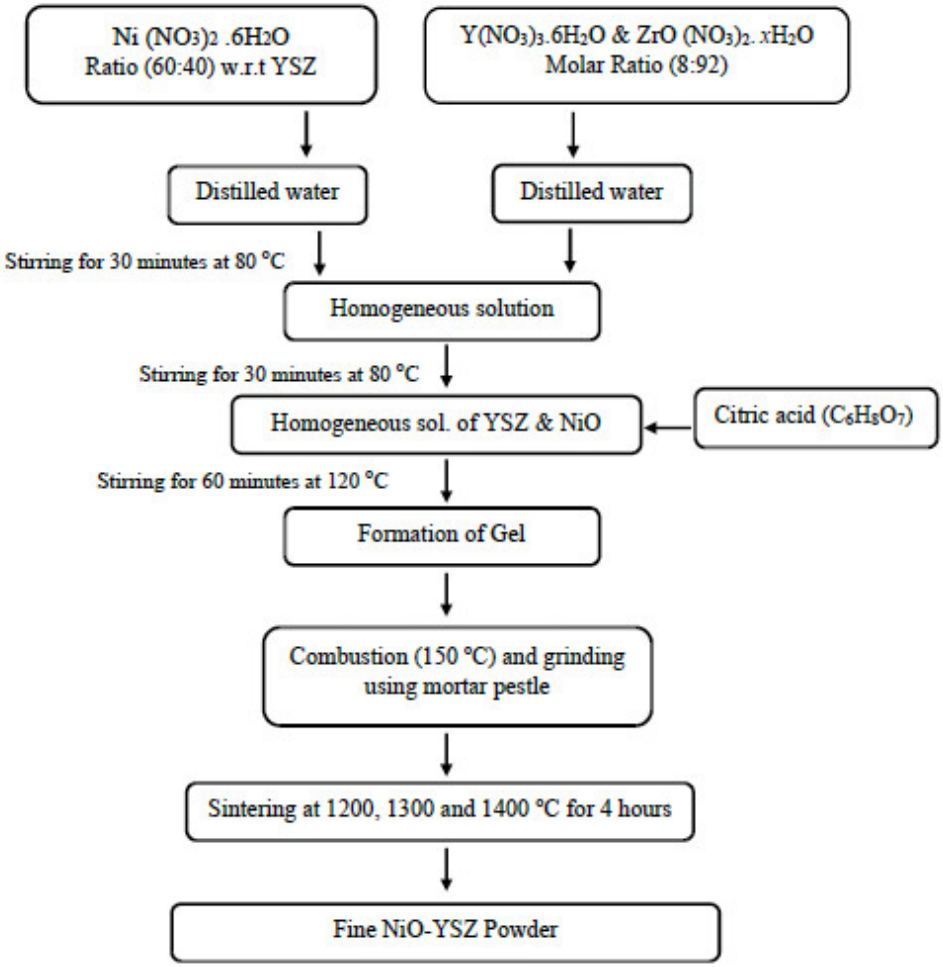

Figure 1. Flow chart of the synthesis of NiO-YSZ.

Cell Fabrication

The electrochemical performance of NiO-YSZ material as an anode, sintered at 1200, 1300, and 1400 °C, was assessed by fabricating three button cells using a hydraulic press. LSM-YSZ and YSZ were used as the cathode and electrolyte materials, respectively. The fabricated cells were sintered for 30 min at 850 °C. Humidified hydrogen (100 mL/min) was used as a fuel and the air was used as an oxidant at the cathode side.

3. Results and Discussion

3.1. Structural Analysis

The diffraction pattern of NiO-YSZ is shown in Figure 2. The Bragg peaks (111), (200), (220), (311), and (222) correspond to the YSZ and (111), (200), and (220) attributed to the crystalline NiO. Diffraction profile analysis confirms single-phase cubic structures of YSZ and NiO by comparing them with the JCPDS card nos. 30-1468 and 01-1239, respectively. The existence of individual peaks of YSZ and NiO and the absence of secondary phases in the diffractogram show that no chemical reaction takes place during synthesis. There is no peak shifting, and therefore the cell volume remains unchanged upon doping.

It is clear from the diffractogram that peaks of YSZ and NiO become more and more intense with the increase in sintering temperature. Hence, the small peak widths are attributed to the improved crystallinity, which is necessary for the enhanced performance of the NiO-YSZ anode-based cell. The crystallite size may increase due to grain growth by heat treatment [22,23]. Crystallite sizes of YSZ and NiO are listed in Table 1.

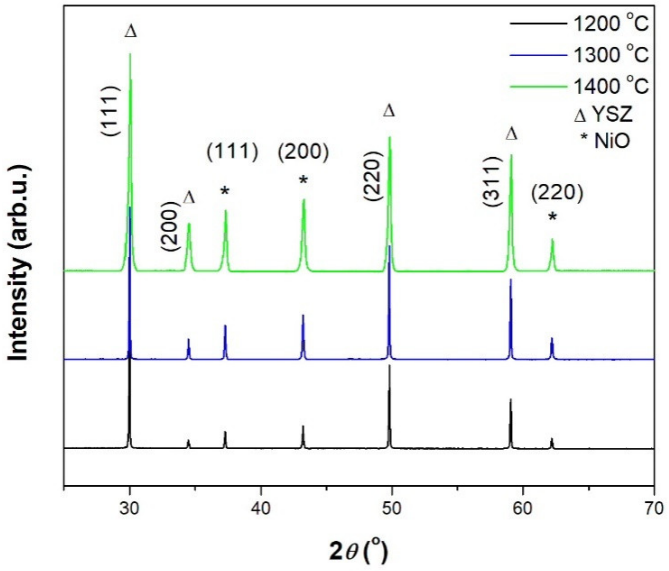

Figure 2. X-ray diffraction pattern of NiO-YSZ anode material sintered at different temperatures.

Table 1. Crystallite size of NiO and YSZ at different sintering temperatures.

Anode Material	Crystallite Size		
	1200 °C	**1300 °C**	**1400 °C**
NiO	12.6 nm	17.94 nm	32.33 nm
YSZ	13.66 nm	21.38 nm	39.03 nm

3.2. Morphology of NiO-YSZ

Figure 3a–c represents the SEM micrographs of NiO-YSZ anode for use in SOFC. A porous structure can be seen in the SEM micrographs shown in Figure 3a. A dense structure with large open pores is presented in Figure 3b, whereas a denser and compact structure is shown in Figure 3c. The comparison shows that the increased sintering temperature caused densification of the material because of increased agglomeration of NiO-YSZ particles. Therefore, an increase in crystallinity along with coarsening of grains leads to better anode performance. A decrease in porosity causes an increased polarization resistance, hence, with decreased porosity, the cell performance decreases [24].

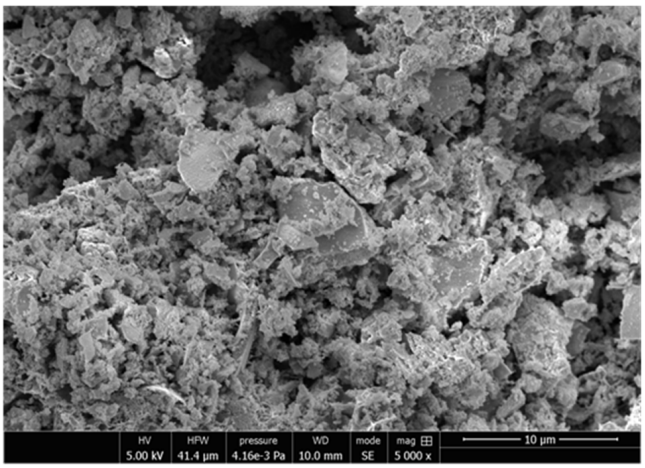

(**a**)

Figure 3. *Cont.*

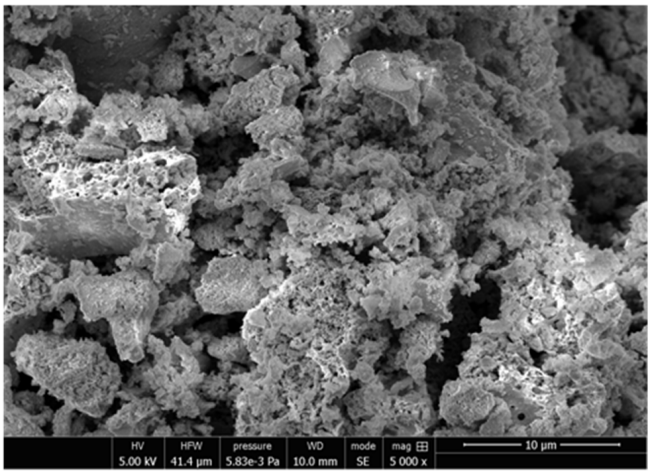

(**b**)

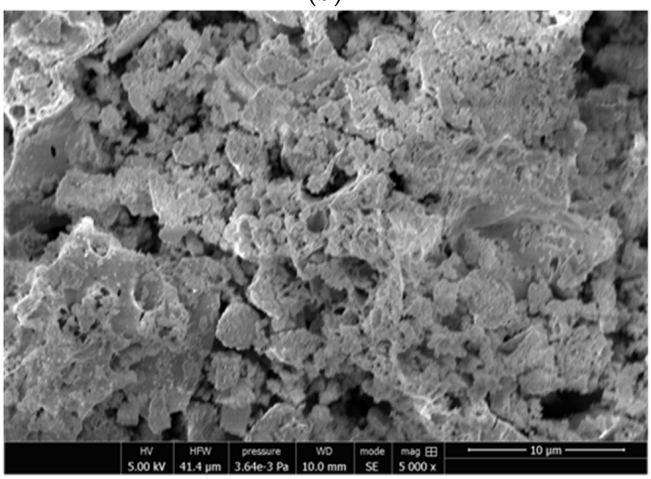

(**c**)

Figure 3. Surface morphology of NiO-YSZ material sintered at (**a**) 1200 °C, (**b**) 1300 °C, and (**c**) 1400 °C.

In the prepared NiO-YSZ, it can be seen that the grain growth, which already started at 1200 °C, continues during sintering treatment till 1400 °C. At 1400 °C, maximum agglomeration of particles has been achieved, and above 1400 °C YSZ material sintering is stopped [25]. Moreover, with increased crystallization during the sintering process, smaller NiO-YSZ particles agglomerate together by getting in contact and stay to form larger particles through extended suitable crystalline orientations, which results in a crystal growth.

3.3. EDX Analysis

Figure 4 depicts the EDX spectrum of NiO-YSZ as an anode material. The EDX spectrum confirms nickel, oxygen, zirconium, and yttrium in the prepared samples. The average elemental composition of zirconium, yttrium, and nickel is 32%, 3%, and 56%, respectively. The presence of nickel and zirconium is also indicated by the XRD analysis. The remaining percentage corresponds to the presence of oxygen due to oxides formation.

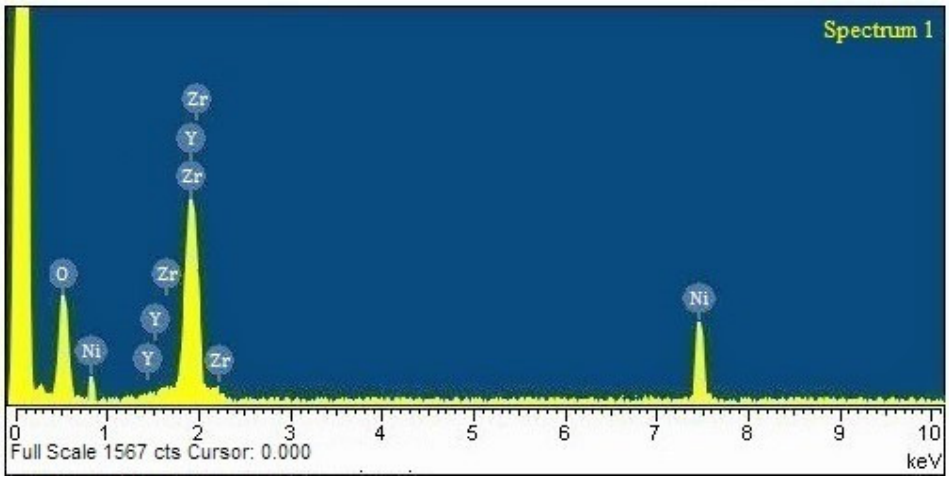

Figure 4. EDX spectrum of pre-sintered NiO-YSZ anode material.

3.4. Thermal Analysis

Thermal analysis of NiO-YSZ, as an anode for SOFC, is presented in Figure 5 to investigate the weight loss and stability during the working of the SOFC device at later stages. The weight loss can be noticed between 30 °C to 800 °C in different regions. The overall weight loss is 16%. In region A (30–400 °C), the loss of weight was because of the evaporation of water, nitrates, and hydroxide. In region B (400–700 °C), the straight line shows that no chemical reaction takes place during this range and in region C (720–800 °C). The decomposition of carbonates caused weight loss [22,26,27].

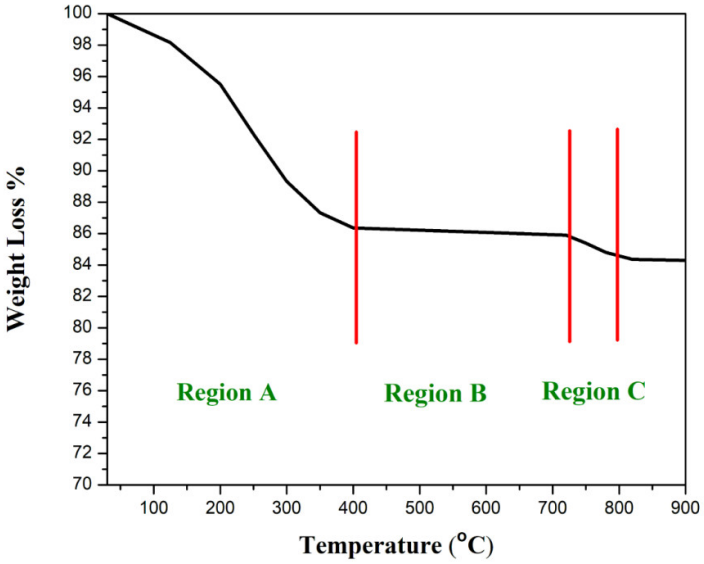

Figure 5. Thermal analysis of the NiO-YSZ anode material.

3.5. Conductivity Measurements

Electronic conductivity measurements of NiO-YSZ cermet, sintered at 1200, 1300, and 1400 °C under the hydrogen atmosphere, are shown in Figure 6. The linear behavior in all three specimens is according to the Arrhenius Equation (4). The Arrhenius plot shows that the conductivity decreased as the temperature increased, which is ascribed as the electronic conductivity of nickel-metal [28]. On the other hand, YSZ is responsible for ionic conductivity. Both Ni and YSZ together govern the net conduction process during the operation of SOFC. The impedance contribution due to the ionic conduction of YSZ also increases with the increased temperature [29].

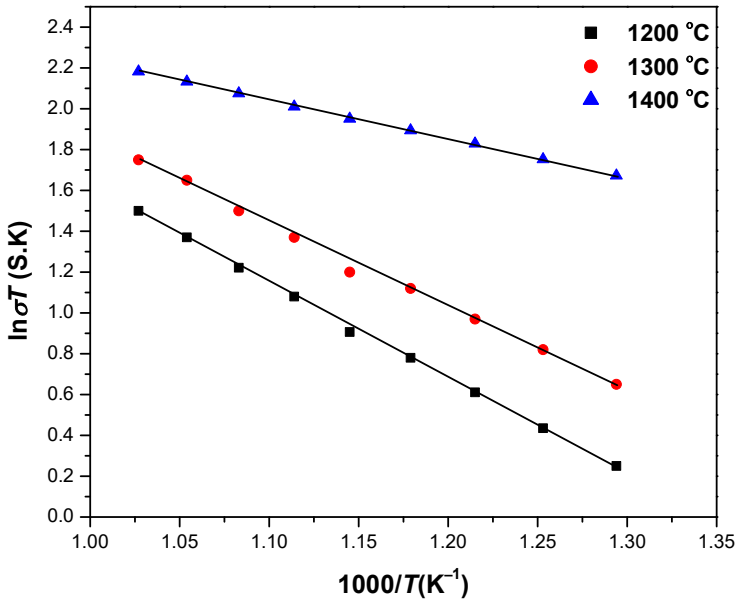

Figure 6. Arrhenius plot of NiO-YSZ anode material sintered at different temperatures.

The SEM analysis proves that an increased sintering temperature formed a dense structure of the anode, which resulted in a decrease in its electronic conductivity. It is also well-known that with the increase in temperature, above 1400 °C, the further grain-growth stops, and grain boundary diffusion increases. This leads to an increase in the length of the TPB [30]. Therefore, the specimen at 1400 °C exhibits high conductivity, which can be attributed to the large triple-phase boundary and minimum polarization resistance. Moreover, the development of the consistent morphology of NiO-YSZ's material is due to the NiO-grains surrounded by the well-distributed YSZ-grains. This further resulted in the formation of a network-structure of NiO-grains, which facilitates the flow of current with stability during the operation of SOFC. The activation energies for the samples sintered at 1200, 1300, and 1400 °C are 0.398 eV, 0.365 eV, and 0.161eV, respectively. The lowest activation energy is observed for the sample sintered at 1400 °C.

3.6. Electrochemical Performance

Figure 7 shows the electrochemical performance of three-button cells having NiO-YSZ as an anode at 800 °C using H_2 as fuel and air as an oxidant at the cathode side. Cells having NiO-YSZ as the anode sintered at 1200, 1300, 1400 °C show peak power densities of 0.44, 0.54, and 0.61 Wcm^{-2} with an open-circuit voltage (OCV) of 0.92, 0.91, and 0.9 V, respectively. It can be observed that cells having NiO-YSZ as the anode sintered at 1400 °C show the highest power density, at 0.61 W/cm^2 with 0.9 V OCV. The NiO-YSZ material sintered at 1400 °C, exhibited a fine and dense structure compared to other samples, also evident from the corresponding SEM micrographs. In addition, the electrical performance is high for the material sintered at 1400 °C.

It is well-known that Ni sinters very easily at temperatures around 1000 °C, but at SOFC-operating temperature the dispersed grains of YSZ on the Ni-surface (after reduction of NiO), do not allow it to become sintered [30]. Therefore, the NiO-YSZ specimen developed at 1200 °C with porous structure delivered a better triple-phase boundary for reaction during SOFC performance. The low value of OCV may be attributed to the potential leakage of gases across the electrolyte due to the existence of any pinhole in the thin electrolyte, as also highlighted elsewhere. Additionally, low OCV may also be a result of lack of gas equilibration in the microporous structures of the electrodes, as pointed out by a group of researchers [31,32].

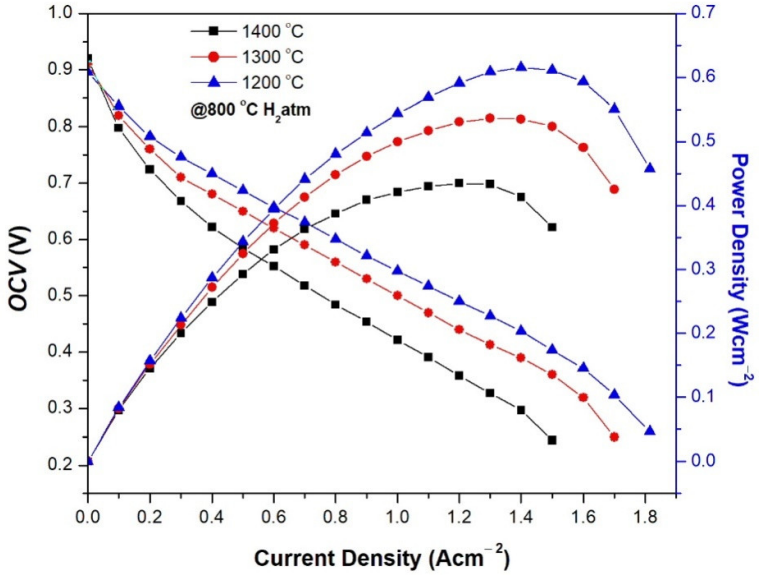

Figure 7. Electrochemical performance of Ni-YSZ cermet at 800 °C.

4. Conclusions

NiO-YSZ was synthesized by the facile combustion method and sintered at 1200, 1300, and 1400 °C. It has been observed that sintering temperatures highly affect the morphology, crystallite size, and conductivity of the end specimens. NiO and YSZ crystallize with cubic symmetry and no secondary phase is observed with improved crystallinity at 1400 °C. The presence of yttria, zirconium, and nickel has been confirmed by EDX and the porous morphology of NiO-YSZ, observed in SEM analysis, was reduced as the temperature increased. The weight loss in the material was 16% for 30–800 °C. The maximum electrochemical performance and power density were achieved for SOFC by sintering the NiO-YSZ anode material at 1200 °C due to its appropriate density, allowing the enhanced electronical reaction at a triple phase boundary.

Author Contributions: Conception and design of project, M.I. (Muneeb Irshad); formal analysis, M.I. (Muneeb Irshad), A.G. and A.N.T.; acquisition of data, M.R., R.R. and A.S.; interpretation of results, M.I. (Muneeb Irshad), Q.u.A. and M.I. (Muhammad Imran); article writing and proof reading, M.I. (Muneeb Irshad), M.I. (Muhammad Imran), K.S. and M.A.A. All authors have read and agreed to the published version of the manuscript.

Funding: This research was funded by King Khalid University grant number [KKU/RCAMS/G015/21].

Data Availability Statement: Data presented in this article are available at request from the corresponding author.

Acknowledgments: The authors especially M. A. Assiri and M. Imran express their appreciation to the Research Center for Advanced Materials Science at King Khalid University, Saudia Arabia through grant number KKU/RCAMS/G015/.

Conflicts of Interest: The authors declare no conflict of interest.

References

1. Fu, Q.; Li, Z.; Wei, W.; Liu, F.; Xu, X.; Liu, Z. Performance enhancement of planar solid oxide fuel cell using a novel interconnector design. *Int. J. Hydrogen Energy* **2021**, *46*, 21634–21656. [CrossRef]
2. Tan, L.; Dong, X.; Chen, C.; Gong, Z.; Wang, M. Diverse system layouts promising fine performance demonstration: A comprehensive review on present designs of SOFC-based energy systems for building applications. *Energy Convers. Manag.* **2021**, *245*, 114539. [CrossRef]
3. Irshad, M.; Idrees, R.; Siraj, K.; Shakir, I.; Rafique, M.; Ain, Q.U.; Raza, R. Electrochemical evaluation of mixed ionic electronic perovskite cathode LaNi1-xCoxO3-δ for IT-SOFC synthesized by high temperature decomposition. *Int. J. Hydrogen Energy* **2021**, *46*, 10448–10456. [CrossRef]
4. Liu, F.; Duan, C. Direct-Hydrocarbon Proton-Conducting Solid Oxide Fuel Cells. *Sustainability* **2021**, *13*, 4736. [CrossRef]

5. Abdelkareem, M.A.; Elsaid, K.; Wilberforce, T.; Kamil, M.; Sayed, E.T.; Olabi, A. Environmental aspects of fuel cells: A review. *Sci. Total Environ.* **2021**, *752*, 141803. [CrossRef] [PubMed]
6. Hussain, S.; Yangping, L. Review of solid oxide fuel cell materials: Cathode, anode, and electrolyte. *Energy Transit.* **2020**, *4*, 113–126. [CrossRef]
7. Irshad, M.; Khalid, M.; Rafique, M.; Tabish, A.N.; Shakeel, A.; Siraj, K.; Ghaffar, A.; Raza, R.; Ahsan, M.; Ain, Q.; et al. Electrochemical Investigations of $BaCe_{0.7-x}Sm_xZr_{0.2}Y_{0.1}O_{3-\delta}$ Sintered at a Low Sintering Temperature as a Perovskite Electrolyte for IT-SOFCs. *Sustainability* **2021**, *13*, 12595. [CrossRef]
8. Inac, S.; Unverdi, S.O.; Midilli, A. A parametric study on thermodynamic performance of a SOFC oriented hybrid energy system. *Int. J. Hydrogen Energy* **2019**, *44*, 10043–10058. [CrossRef]
9. Aman, N.A.M.N.; Muchtar, A.; Somalu, M.R.; Rosli, M.I.; Kalib, N.S. Overview of Computational Fluid Dynamics Modelling in Solid Oxide Fuel Cell. *J. Adv. Res. Fluid Mech. Therm. Sci.* **2018**, *52*, 174–181.
10. Welander, M.M.; Zachariasen, M.S.; Hunt, C.D.; Sofie, S.W.; Walker, R.A. Operando Studies of Redox Resilience in ALT Enhanced NiO-YSZSOFC Anodes. *J. Electrochem. Soc.* **2018**, *165*, F152–F157. [CrossRef]
11. Kim, J.W.; Bae, K.; Kim, H.J.; Son, J.W.; Kim, N.; Stenfelt, S.; Prinz, F.B.; Shim, J.H. Three-dimensional thermal stress analysis of there-oxidized Ni-YSZ anode functional layer in solid oxide fuel cells. *J. Alloys Compd.* **2018**, *752*, 148–154. [CrossRef]
12. Li, F.; Zhang, J.; Luan, J.; Liu, Y.; Han, J. Preparation of Bi_2O_3-DopedNio/Ysz Anode Materials for Sofcs. *Surf. Rev. Lett.* **2017**, *24*, 1750092. [CrossRef]
13. Abdalla, A.M.; Hossain, S.; Azad, A.T.; Petra, P.M.I.; Begum, F.; Eriksson, S.G.; Azad, A.K. Nanomaterials for solid oxide fuel cells: A review. *Renew. Sustain. Energy Rev.* **2018**, *82*, 353–368. [CrossRef]
14. Pihlatie, M.H.; Frandsen, H.L.; Kaiser, A.; Mogensen, M. Continuum mechanics simulations of NiO/Ni-YSZ composites during reduction and re-oxidation. *J. Power Sources* **2010**, *195*, 2677–2690. [CrossRef]
15. Wang, F.H.; Guo, R.S.; Wei, Q.T.; Zhou, Y.; Li, H.L.; Li, S.L. Preparation and properties ofNi/YSZ anode by coating precipitation method. *Mater. Lett.* **2004**, *58*, 3079–3083. [CrossRef]
16. Irshad, M.; Siraj, K.; Raza, R.; Ali, A.; Tiwari, P.; Zhu, B.; Rafique, A.; Ali, A.; Kaleem Ullah, M.; Usman, A. A Brief Description of High Temperature Solid Oxide Fuel Cell's Operation, Materials, Design, Fabrication Technologies and Performance. *Appl. Sci.* **2016**, *6*, 75. [CrossRef]
17. Drożdż, E.; Wyrwa, J.; Rękas, M. Influence of sintering temperature and aging on properties of cermet Ni/8YSZ materials obtained by citric method. *Ion* **2013**, *19*, 1733–1743. [CrossRef]
18. Ojeda, M.; Zhao, T.; Wang, H.; Xuan, J. Ni-YSZ Nanocomposite Synthesis: Mechanochemical vs. Novel Sol-Gel Method for Solid Oxide Electrolysers. *Energy Procedia* **2017**, *142*, 1095–1099. [CrossRef]
19. Grgicak, C.M.; Green, R.G.; Du, W.F.; Giorgi, J.B. Synthesis and characterization of NiO-YSZ anode materials: Precipitation, calcination, and the effects on sintering. *J. Am. Ceram. Soc.* **2005**, *88*, 3081–3087. [CrossRef]
20. Hargreaves, J.S.J. Some considerations related to the use of the Scherrer equation in powder X-ray diffraction as applied t heterogeneous catalysts. *Catal. Struct. React.* **2016**, *2*, 33–37. [CrossRef]
21. Nityanand, C.; Nalin, W.B.; Rajkumar, B.S.; Chandra, C.M. Synthesis and physicochemical characterization of nanocrystalline cobalt doped lanthanum strontium ferrite. *Solid State Sci.* **2011**, *13*, 1022–1030. [CrossRef]
22. Park, S.Y.; Na, C.W.; Ahn, J.H.; Song, R.H.; Lee, J.H. Preparation of highly porous NiO-gadolinium-doped cerianano-composite powders by one-pot glycine nitrate process for anode-supported tubular solid oxide fuel cells. *J. Asian Ceram. Soc.* **2014**, *2*, 339–346. [CrossRef]
23. Zhu, X.; Lü, Z.; Wei, B.; Huang, X.; Zhang, Y.; Su, W. Asymmetrical solid oxide fuel cell prepared by dry-pressing and impregnating methods. *J. Power Sources* **2011**, *196*, 729–733. [CrossRef]
24. Ahsan, M.; Irshad, M.; Fu, P.F.; Siraj, K.; Raza, R.; Javed, F. The effect of calcination temperature on the properties of Ni-SDC cermet anode. *Ceram. Int.* **2020**, *46*, 2780–2785. [CrossRef]
25. Solovyev, A.A.; Ionov, I.V.; Kovalchuk, A.N.; Kirdyashkin, A.I.; Maznoy, A.S.; Kitler, V.D. Sintering ofnio/ysz anode layers for metal-supported solid oxide fuel cell. *Adv. Mater. Res.* **2014**, *1040*, 155–160. [CrossRef]
26. Irshad, M.; ul Ain, Q.; Siraj, K.; Raza, R.; Tabish, A.N.; Rafique, M.; Idrees, R.; Khan, F.; Majeed, S.; Ahsan, M. Evaluation of$BaZr_{0.8}X_{0.2}$ (X = Y, Gd, Sm) proton conducting electrolytes sintered at low temperature for IT-SOFC synthesized by cost effective combustion method. *J. Alloys Compd.* **2020**, *815*, 152389. [CrossRef]
27. Irshad, M.; Siraj, K.; Raza, R.; Rafique, M.; Usman, M.; ul Ain, Q.; Ghaffar, A. Evaluation of densification effects on the properties of 8 mol% yttria stabilized zirconia electrolyte synthesized by cost-effective coprecipitation route. *Ceram. Int.* **2020**, *47*, 2857–2863. [CrossRef]
28. Han, K.R.; Jeong, Y.; Lee, H.; Kim, C.S. Fabrication of NiO/YSZ anode material for SOFC via mixed NiO precursors. *Mater. Lett.* **2007**, *61*, 1242–1245. [CrossRef]
29. Bueta, F.R.; Imperial, J.F.; Cervera, R.B. Structure and conductivity of NiO/YSZ composite prepared via modified glycine-nitrate process at varying sintering temperatures. *Ceram. Int.* **2017**, *43*, 16174–16177. [CrossRef]
30. Fukui, T.; Ohara, S.; Naito, M.; Nogi, K. Performance and stability of SOFC anode fabricated from NiO/YSZ composite particles. *J. Eur. Ceram. Soc.* **2003**, *23*, 2963–2967. [CrossRef]
31. Chiodelli, G.; Malavasi, L. Electrochemical open circuit voltage (OCV) characterization of SOFC materials. *Ionics* **2013**, *19*, 1135–1144. [CrossRef]
32. Jin, C.; Yang, C.; Chen, F. Effects on microstructure of NiO—YSZ anode support fabricated by phase-inversion method. *J. Membr. Sci.* **2010**, *363*, 250–255. [CrossRef]